sciendo

ACTA CHEMICA IASI, **27_1**, 73-86 (2019)

DOI: 10.2478/achi-2019-0006

SYNTHESIS AND CHARACTERIZATION OF $Co_{0.8-x}Ni_xZn_{0.2}Fe_2O_4$ FERRITES BY WILLIAMSON–HALL AND SIZE–STRAIN PLOT METHODS

Ravikumar Kolekar[a], Suresh Baburao Kapatkar[b*], Shridhar Narasinhmurthy Mathad[c†]

[a]*Department of Physics, M.E.S.M.M Arts and Science College Sirsi, India*

[b]*Department of Physics, KLE Technological University (KLE Tech), Vidyanagar, Hubballi, India*

[c]*Department of Physics, K.L.E.I.T., Hubballi, India*

Abstract: The Co-Zn ferrite (x=0.00) and Nickel doped Co-Zn ferrites (x=0.24) was synthesized by low cost solid state reaction method and characterized by XRD technique. The X-ray diffraction results for the samples showed the formation of single phase cubic spinel. The lattice constant and particle size for Co-Zn ferrite(x=0.00) is found to be 8.3465 Å and 26.72 nm and for Nickel doped (x=0.24) it is 8.3440 Å and 24.21nm. Micro strain (**ε**), Dislocation density(ρ_D), Hopping lengths (L_A and $L_{B)}$,Bond lengths (A - O and B-O), Ionic radii (r_A and r_B), Texture coefficients (T_{hkl}) and Standard deviation (σ) are also reported. The particle size is confirmed by scanning electron microscope (SEM). The Williamson-Hall plot and stress-strain plot also employed to understand the mechanical properties of materials.

***Keywords*:** Co-Zn ferrite, Solid state reaction method, XRD, Texture coefficients, and SEM

[*] Suresh Baburao Kapatkar, *e-mail:* sbkapatkar@bvb.edu

[†] Shridhar Narasinhmurthy Mathad, *e-mail:* physicssiddu@gmail.com

Introduction

Magnetic materials which have combined electrical and magnetic properties are known as ferrites.[1] Iron oxide and metals oxides are the main constituents of the ferrites. Ferrite materials are insulating magnetic oxides and possess high electrical resistivity, low eddy current and dielectric losses, high saturation magnetization, high permeability and moderate permittivity. No material with such wide ranging properties exists and therefore ferrites are unique magnetic materials which find applications in almost all fields. Ferrites are highly sensitive to preparation method, sintering condition, amount of constituent metal oxides, various additives include dopants and impurities.[2-4] Ferrites are of great technological importance by virtue of their interesting electrical and magnetic properties. They are used in transformer cores, antenna rods, memory chips, high density magnetic recording media, permanent magnets, transducers, activators, microwave, medical field and computer technology.[5-7]

Cobalt ferrite ($CoFe_2O_4$) has inverse spinel structure with Co^{2+} ions in octahedral site and Fe^{3+} ions equally distributed between tetrahedral and octahedral site. It possesses excellent chemical stability, good mechanical hardness and a large positive first-order crystalline anisotropy constant, which made this ferrite a promising candidate for magneto-optical recording media, biological applications, including magnetic resonance imaging (MRI), magnetic fluid, hyperthermia (MFH), magnetic separations, and biosensors, targeted and controlled drug delivery. Numerous method have been employed for synthesizing ferrite particles such as Co-precipitation,[8] Combustion and microwave method,[9] solvothermal method,[10] citrate precursor,[11] solid state reaction method[12] and sol–gel method.[13]

Many researchers explored structural characteristics of zinc ferrite,[16] Li-Ni-Zn ferrite,[17] Li-doped magnesium zinc ferrite,[18] Cadmium doped Ni–Zn ferrites,[19] Zn sub of Co ferrite,[20] Al sub of Co-Zn ferrite,[21] and Cr sub of Co-Zn ferrite.[22]

Regardless of many studies, the influence of nickel doping on structural, electrical, magnetic and optical properties of Co-Zn spinel ferrites have not been reported so far. It finds applications in the electronics and microwave devices due to their high electrical resistivity, low eddy current and dielectric loss.[23]

In this studies we report, methodology of synthesis of Nickel doped Co-Zn ferrite based on the low cost solid state reaction method. A detailed structural characterization of sample was understood by XRD technique and the morphology by SEM.

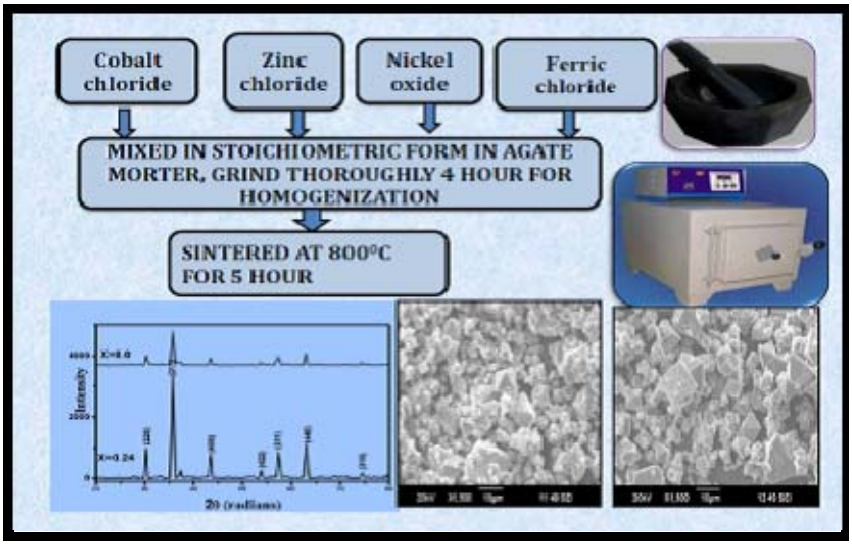

Figure1. Schematic diagram of synthesis of $Co_{0.8-x}Ni_xZn_{0.2}Fe_2O_4$ ferrite by solid state reaction method.

Experimental

All the starting materials of analytical grade (Kemphasol) $CoCl_2 \cdot 6H_2O$, $ZnCl_2$, $FeCl_3$ anhydrous and NiO were thoroughly mixed, in stichiometric proportions acetone with a pestle in a mortar. The reaction mass was transferred in a crucible and preheated at a temperature of 250°C for 2 to 3 hours. The mixture was finely powdered and heated in a muffle furnace(Mechanical work shop, B.V.B. College, Hubballi) at gradually increasing temperatures of 60, 100, 200, 600 and 800°C for 5 hours (shown in Figure 1). Structural characterization of ferrite powders was carried out by using Bruker AXS D8 Advance diffractometer (Cu-Kα radiation, wavelength=1.5406Å) and particle size by SEM.

The structural characteristics of Co-Zn ferrite (x=0.00) and Nickel doped Co-Zn ferrite (x=0.24) particles are determined by the aid of X-ray diffraction (XRD) (Bruker AXS D8 Advance model diffractometer Cu-Kα radiation, wavelength λ=1.5406Å). The morphology of the prepared sample is examined by Scanning electron microscope (SEM)(JEOL Model JSM-6390LV).

Results and Discussion

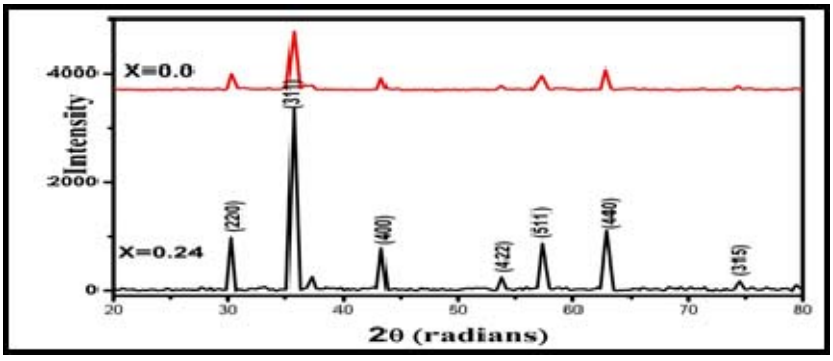

Figure 2. XRD pattern of $Co_{0.8-x}Ni_x\,Zn_{0.2}\,Fe_2O_4$ ferrite.

X-ray diffraction analysis

The XRD patterns of Co-Zn(x=0.00) ferrite and Nickel doped Co-Zn ferrite (x=0.24) particles are presented in Figure 2.

For pure Co-Zn ferrite (x=0.00) the diffraction pattern analysis by using the (220), (311), (400), (422), (511) and (440) reflection plane confirms a cubic spinel structure. For Nickel doped Co-Zn ferrite (x=0.24) the diffraction pattern analysis by using the (220), (311), (400), (422), (511) and (440) reflection plane also confirms a cubic spinel structure.

The peaks position and relative intensity matches with the standard (JCPDC card 00-001-1121). This proves that synthesized sample belongs to cubic spinel structure with lattice constant 8.3465 Å (x=0.00) and 8.3440 Å (x=0.24).

Average crystallites size (D) is calculated using the Debye-Scherrer formula.[24]

$$D = \frac{0.9\lambda}{\beta \cos\theta} \tag{1}$$

Where λ is the wavelength of X-rays (1.5406 Å) and θ is Bragg's angle for a given peak. The accuracy of this equation is subject to the error limitations of crystallite shape factor K and purely diffraction broadening β. The value of K is taken 0.9 in present case. The distance between magnetic ions (hopping length) in A site (Tetrahedral) and B site (Octahedral) (L_A and L_B) were calculated by using the following relations (2, 3).[25]

$$L_A = \frac{a \times \sqrt{3}}{4} \tag{2}$$

$$L_B = \frac{a \times \sqrt{2}}{4} \tag{3}$$

The bond lengths (A–O and B–O) and ionic radii (r_A and r_B) on A-site and B-site are calculated using the following equation (4-7) and are presented in Table 1.

$$A-O=(u-1/4)a\sqrt{3} \quad (4)$$

$$B-O=(5/8-u)a \quad (5)$$

$$r_A=(u-1/4)a\sqrt{3}-r(O^{2-}) \quad (6)$$

$$r_B=(5/8-u)a-r(O^{2-}) \quad (7)$$

Table 1. Calculated value of Lattice parameter (a), Volume of unit cell (V), Hopping length (L_A and L_B), Bond length (A-O, B-O) and Ionic radii (r_A and r_B).

X	**a (Å)**	**V (Å^3)**						
			L_A (Å)	**L_B (Å)**	**A-O (Å)**	**B-O (Å)**	**r_A (Å)**	r_B (Å)
0.00	8.3465	581.45	3.6141	2.9509	1.8071	2.0866	0.4571	0.7366
0.24	8.3440	580.93	3.6131	2.9500	1.8065	2.0860	0.4565	0.7360

The dislocation is a crystallographic defect in a crystal structure. It plays a very important role in understanding the influence of defects on properties of materials at macro level. The dislocation density gives total number of dislocations (ρ_D) per unit volume of the material.[26] The dislocation density helps in interpreting total defects. The following relations (8-10) are used to calculate micro strain (**ε**) in the crystal and dislocation density (ρ_D). The results are tabulated in Tables 2 and 3.

$$micro-strain(\varepsilon)=\frac{\beta\cos\theta}{4} \quad (8)$$

Dislocation Density (ρ_D)

$$(\rho_D) = \frac{1}{D^2} \tag{9}$$

$$\rho_D = \frac{15\varepsilon}{aD} \tag{10}$$

Table 2. Calculation of Crystallite size (D), Dislocation density (ρ_D) and Micro strain (**ε**) from formula, for x = 0.00.

Sl. No.	**Angle 2θ (°)**	**FWHM β (°)**	**D (Å)**	**ρ_D ($\times 10^{15}$ m^{-2})**	**ε**
1	30.318	0.375	219.41	2.0773	0.001580
2	35.677	0.373	223.66	1.9990	0.001550
3	43.331	0.382	223.70	1.9983	0.001550
4	53.710	0.306	290.92	1.1816	0.001192
5	57.216	0.289	313.03	1.0206	0.001107
6	62.814	0.280	332.34	0.90536	0.001043
9		**Average**	**267.22**	**1.5303 X10^{15}**	**0.001337**

Table 3. Calculation of Crystallite size (D), Dislocation density (ρ_D) and Micro strain (**ε**) from formula, for x = 0.24.

Sl. No.	**Angle 2θ**	**FWHM β (in degrees)**	**D (Å)**	**ρD X10^{15} m^{-2}**	**ε**
1	30.296	0.323	254.72	1.5413	0.001361
2	35.64	0.326	255.90	1.5271	0.001355
3	43.362	0.341	250.62	1.5920	0.001383
4	53.759	0.379	234.93	1.8118	0.001475
5	57.301	0.396	228.54	1.9146	0.001517
6	62.922	0.408	228.21	1.9201	0.001519
		Average	242.15	1.7178 X10^{15}	0.001435

Texture analysis

The reflection intensities from each XRD pattern contain information related to the preferential or random growth of polycrystalline material, which is studied by calculating texture coefficient TC (hkl) for all planes using the formula (11)[26].

$$TC(hkl) = \frac{I(hkl)/I_0(hkl)}{\left(\frac{1}{n}\right)\sum I(hkl)/I_0(hkl)} \qquad (11)$$

where I (hkl) is the measured intensity of X-ray reflection, I_0 (hkl) is the corresponding standard intensity from the JCPDC card 00-001-1121, and N is the number of reflections observed in the XRD pattern. Table 4 shows variation in the TC of different (hkl) values.

Table 4. Calculated values of TC for different (hkl) values.

Sl. No	Miller indices			Texture analysis	
	h	k	l	TC X=0.0	TC X=0.24
1	2	2	0	1.5347	1.5469
2	3	1	1	1.5768	1.5838
3	4	0	0	0.8554	0.9225
4	4	2	2	0.6465	0.6018
5	5	1	1	0.6753	0.6837
6	4	4	0	0.7116	0.6612

Texture coefficient is higher than 1 indicates preferential orientation and also indicates the abundance of grains along the given (hkl) plane. This is fact that, the values of (220) and (311) are relatively higher value than

other planes indicating higher orientations of crystallites along the (220) and (311) planes.

Scanning Electron Microscope Analysis:

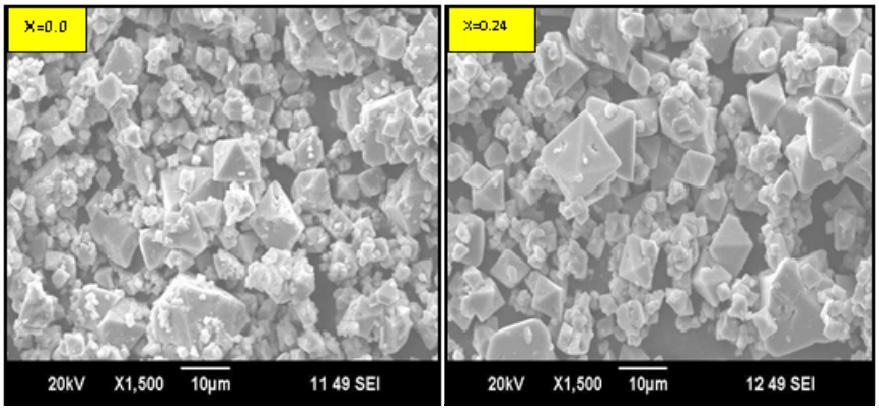

Figure 3. SEM image of x = 0.00 and x = 0.24.

The SEM is widely used to identify phases based on qualitative chemical analysis and crystalline Structure. Back scattered electron images can be used for rapid discrimination of phases in multiphase samples. The SEM analysis was carried out to investigate the detailed morphology of the synthesized pure Co-Zn ferrite(x=0.00) and Nickel doped Co-Zn ferrites (x = 0.24) with dopant concentration as shown in Figure 3. The micro structure of ferrites observed average grain sizes are 2.85µm to 2.35µm.

Size-strain plot and Williamson -Hall plot [28-30]

Lattice strain η and average crystalline size *D* were calculated using the Williamson–Hall equation. [28-30]

$$\frac{\beta\cos\theta}{\lambda} = \frac{1}{D} + \frac{\eta\sin\theta}{\lambda} \qquad (12)$$

The above equation is written in the format $y = mx + c$ where $m = \eta$ and $c = 1/D$, so that the linear plot of βcos θ vs. sin θ gives the slope as lattice strain η and the intercept as 1/D as shown in Figure 4. Figure 5 represents the size-strain plots of ferrite samples. From the graph calculated average crystallite size (*D)* and lattice strain to agree with both analysis (SSP and W-H Plots).

Accordingly, we have [28-30]

$$(d_{hkl}\beta_{hkl}\cos\theta)^2 = \frac{K.\lambda}{D}(d_{hkl}^2\beta_{hkl}\cos\theta) + \left(\frac{\varepsilon}{2}\right)^2 \quad (13)$$

where K is a constant that depends on the shape of the particles (for spherical particles K= 3/4).

In this case, the comparison of all parameters between W-H plot and SSP has been reported in Table 5.

Table 5. Comparative values of crystallite size (D), micro strain (ε), and dislocation density (ρ_D).

x	**0.00**				**0.24**			
D (Å)	From equation	From graph	W-H	From SSP method	From equation	From graph	W-H	From SSP method
	267.22	111		320	242.15	218		219
ε	From equation	From graph	W-H	From SSP method	From equation	From graph	W-H	From SSP method
	0.001337	0.0092		0.0099	0.001435	0.00458		0.00704
ρ_D (m^{-2})	From eqn	From eqn			From eqn	From eqn		
	1.5303 $X10^{15}$	1.75 $X10^{15}$			1.7178 $X10^{15}$	1.85 $X10^{15}$		

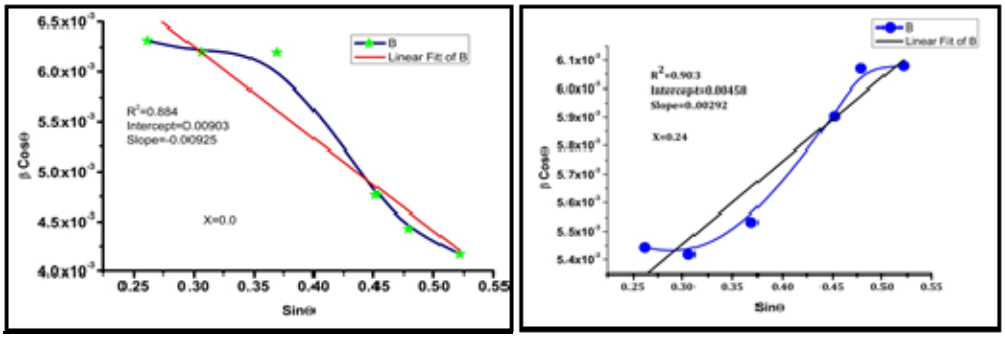

Figure 5. Williamson–Hall plot of βcosθ vs. sinθ.

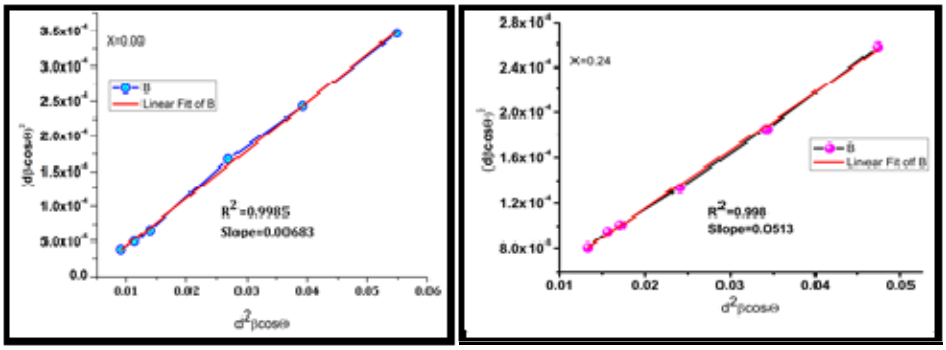

Figure 6. Size-strain plot of Nickel doped Co-Zn ferrites.

Conclusion:

$Co_{0.8-x}Ni_x Zn_{0.2}Fe_2O_4$ (X=0.0, 0.24) ferrites were synthesized from solid state method confirmed spinal cubic structure from x-ray diffraction analysis. Texture coefficients analysis indicates that, the grain growth is relatively higher orientations of crystallites along the (220) and (311) planes. SEM analysis shows that the particles are crystalline in nature. SEM images shows regular octahedron and bead like structured grains with grain size more than 2.35µm. We have also compared the crystalline structure by W-H plot and SSP method.

References

1. Smit, J. and Wijn, H.P.J., *Ferrites*. Philips Technical Library, Eindhoven, 1959.

2. Gadkari, A.B.; Shinde, T.J.; Vasambekar, P.N. Structural analysis of Y^{3+}-doped Mg–Cd ferrites prepared by oxalate co-precipitation method. *Mater. Chem. Phys.* **2009**, *114,* 505-510.

3. Gama, L.; Diniz, A.P.; Costa, A.C.F.M.; Bezende, S.M.; Azevedo, A.; Cornejo, D.R. Magnetic properties of nanocrystalline Ni–Zn ferrites doped with samarium. *Physica B: Conden. Matter*. **2006**, *384*, 97-99.

4. Jcoba, S.E.; Dukalde, S.; Bertorella, H.R. Rare earth influence on the structural and magnetic properties of NiZn ferrites. *J. Magn. Magn. Mater*. **2004**, *272*, 2253-2254.

5. Verma, A.; Goel, T.C.; Mendiratta, R.G.; Gupta, R.G. High-resistivity nickel–zinc ferrites by the citrate precursor method. *J. Magn. Magn. Mater*. **1999**, *192*, 271-276.

6. Nakamura, T.; Miyamoto, T.; Yamada, Y. Complex permeability spectra of polycrystalline Li–Zn ferrite and application to EM-wave absorber. *J. Magn. Magn. Mater*. **2003**, *256*, 340-347.

7. Waqus, H.; Quresghi, A.H. Influence of pH on nanosized Mn-Zn ferrite synthesized by sol-gel auto combustion process. *J. Therm. Anal. Calorim*. **2009**, *98*, 355-360.

8. Yattinahalli, S.S.; Kapatkar, S.B.; Mathad, S.N. Synthesis and structural characterization of nano manganese ferrites. *J. Nano- Electron. Phys.* **2015**, *7*(4), 0496-1-0496-3.

9. Molakeri, A.S.; Mathad, S.N.; Structural analysis of nano ferrites synthesized by combustion and microwave methods. *Int. J. Self-Propag. High. Temp. Synth.* **2018**, *27*, 44-50.

10. Karpagavalli, S.; Pathamanathan, J.K.; Perumal, S; Koilpillai, D.P.; Suganth, A. A comparative study of optical and magnetic properties of undoped and cobalt doped manganese oxide nano particles. *IOSR J. Appl. Phys.* **2017**, 34-42. DOI10.9790/4861-17002013442

11. Sileoa, E.E.; Rotelob, R.; Jacobo, S.E. Nickel zinc ferrites prepared by the citrate precursor method. *Physica B* **2002**, *320*, 257-260.

12. Kulkarni, A.B.; Mathad, S.N. Synthesis and structural analysis of Co-Zn-Cd ferrite by Williamson–Hall and Size-Strain Plot Method. *Int. J. Self-Propag. High. Temp. Synth*. **2018**, *27*, 37-43.

13. Shirsath, S.E. ; Kadam, R.H.; Gaikwad, A.S.; Ghasemi, A.; Morisako, A. Effect of sintering temperature and the particle size on the structural and magnetic properties of nanocrystalline $Li_{0.5}Fe_{2.5}O_4$. *J. Magn. Magn. Mater*. **2011**, *323*, 3104-3108.

14. Franco, A.; Silva, F.C. Effect of the Zn content in the magnetic properties of $Co_{1-X}\ Zn_x\ Fe_2O_4$ mixed ferrites. *J. App. Phys.* **2013**, *113*, 17b513.

15. Pal, M.; Brahma, P.; Chakravorthy, D. Magnetic and electrical properties of nickel-zinc ferrites doped with bismuth oxide. *J. Magn. Magn. Mater*. **1996**, *152*, 370-374.

16. Yattinahalli, S.S.; Mathad, S.N.; Kapatkar, S.B. Structural studies of zinc ferrite synthesized at low temperature, *Int. Rev*., **2014**, *1(1)*, 5–8.

17. Pathan, A.T.; Mathad, S.N.; Shaikh, A.M. Infrared spectral studies of Co^{2+} substituted Li -Ni-Zn ferrites. *Int. J. Self - Propag. High. Temp. Synth.* **2014**, 23(2), 112–117.

18. Rendale, M.K.; Mathad, S.N.; Puri, V. Thick films of magnesium zinc ferrite with lithium substitution: Structural characteristics. *Int. J. Self-Propag. High. Temp. Synth*. **2015**, *24(*2), 78-82.

19. Patil, M.R.; Rendale, M.K.; Mathad, S.N.; Pujar, R.B. Structural and IR study of $Ni_{0.5-x}Cd_xZn_{0.5}Fe_2O_4$. *Int. J. Self - Propag. High. Temp. Synth*. **2015**, *24(4)*, 241–245.

20. Somaiah, N.; Jayaraman, T.V.; Joy, P.A.; Das, D. Magnetic and magneto elastic properties of Zn-doped cobalt-ferrites $CoFe_{2-x}Zn_xO_4$ (x = 0, 0.1, 0.2, and 0.3). *J. Magn. Magn. Mater*. **2012**, *324*(14), 2286–2291.

21. Singhal, S.; Sharma, R.; Namgyal, T.; Jauhar, S.; Bhukal, S.; Kaur, J. Structural, electrical and magnetic properties of $Co_{0.5}Zn_{0.5}Al_xFe_{2-x}O_4$ (x = 0, 0.2, 0.4, 0.6, 0.8, and 1.0) prepared via sol–gel route. *Ceram. Int*. **2012**, *38*, 2773–2778.

22. Bhukal, S.; Namgyal, T.; Mor, S.; Bansal, S.; Singhal, S. Structural, electrical, optical and magnetic properties of chromium substituted Co–Zn nanoferrites $Co_{0.6}Zn_{0.4}Cr_xFe_{2-x}O_4$ ($0 \leq x \leq 1.0$) prepared via sol–gel auto-combustion method. *J. Mol. Struct.* **2012**, *1012*, 162–167.

23. Stppples, D. Developments in soft magnetic power ferrite, *J. Magn. Magn. Mater*. **1996**, , 323-328.

24. Yattinahalli, S.S.; Kapatkar, S.B.; Ayachit, N.H.; Mathad, S.N. *Int. J. Self. - Propag. High Temp. Synth*. **2013**, *22*, 147-150.

25. Shedam, R.M.; Gadkari, A.B.; Mathad. S.N., Shedam, M.R. Structural and mechanical properties of nanograined magnesium ferrite produced by oxalate coprecipitation method. *Int. J. Self - Propag. High. Temp. Synth.* **2017**, *26*, 75-79.

26. Mathad, S.N.; Jadhav, R.N.; Phadtare, V.; Puri. V. Structural and mechanical properties of Sr-doped barium niobate thick films. *Int. J. Self - Propag. High. Temp. Synth.* **2014**, *23*, 145-150.

27. Babar, A.R.; Shinde, S.S.; Moholkar, A.V.; Bhosale, J.; Kim, H.; Rajpure, K.Y. Physical properties of sprayed antimony doped tin oxide thin films: The role of thickness. *J. Semicond.* **2011**, *32(5)*, 053001–053008.

28. Prabhu, Y.T.; Rao, K.V.; Kumar, V.S.S.; Kumari, B.S. X-ray analysis by Williamson-Hall and size-strain plot methods of ZnO nano particles with fuel variation. *World J. Nano Sci. Eng.* **2014**, *4*, 21–28.

29. Mathad S.N. Mechanical and structural properties of $Zn_{0.1}Ni_{0.4}Cu_{0.5}Fe_2O_4$ ferrite, *Int. J. Adv. Sci. Eng.* **2018**, *5(2)*, 911-916.

30. Shashidhargouda, H.R. Mathad, S.N. Synthesis and structural analysis of $Ni_{0.45}Cu_{0.55}Mn_2O_4$ by Williamson–Hall and size–strain plot methods. *Ovidius University Annals of Chemistry* **2018**, *29*(2), 122-125.